Comparative study of Ganoderma lucidum hydrocolloids from fruiting bodies and liquid fermentation : Structural characterization and different interactions with gluten networks

Food Hydrocolloids

Xu, Zhuojia; Ngadze, Ruth T.; Shen, Jie; Linnemann, Anita R.; Wu, Fengfeng et al

https://doi.org/10.1016/j.foodhyd.2025.111840

Food Hydrocolloids 171 (2026) 111840

Contents lists available at ScienceDirect

Food Hydrocolloids

journal homepage: www.elsevier.com/locate/foodhyd

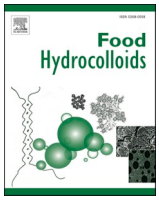

Comparative study of *Ganoderma lucidum* hydrocolloids from fruiting bodies and liquid fermentation: Structural characterization and different interactions with gluten networks

Zhuojia Xu [a,b,c], Ruth T. Ngadze [c], Jie Shen [a,d], Anita R. Linnemann [c], Fengfeng Wu [a,b], Dan Xu [a,b], Jianmei Luan [e,**], Xueming Xu [a,b,*]

[a] School of Food Science and Technology, Jiangnan University, 1800 Lihu Road, Wuxi, 214122, PR China
[b] Anqing Yixiu Green Food Innovation Research Institute, Anqing, PR China
[c] Food Quality & Design Group, Wageningen University & Research, Wageningen, the Netherlands
[d] Tramy Group Co., Ltd, Shanghai, 201399, PR China
[e] Wuxi COFCO Engineering & Technology Co. , Ltd, Wuxi, 214035, PR China

ARTICLE INFO

Keywords:
Ganoderma lucidum
Proteoglycan
Polysaccharides
Structure characterization
Gluten structure
Interaction

ABSTRACT

Hydrocolloids are widely utilized in the food industry as functional additives to enhance product physical quality, such as improving dough handling, strengthening gluten networks, retaining moisture, and enhancing texture in bread and other cereal-based products. This study assessed the structural and functional properties of *Ganoderma lucidum* polysaccharides (GLPs, extracted from fruiting bodies) and proteoglycans (GLPg, obtained via liquid fermentation), focusing on their different hydrophobicity drives interactions in gluten networks during formation. Due to the presence of peptide components, GLPg exhibited significantly higher surface hydrophobicity than GLPs, as confirmed by Fourier transform infrared spectroscopy and circular dichroism. This difference in hydrophobicity played a crucial role in modulating their interactions with gluten proteins. The incorporation of GLPs or GLPg into gluten dough (termed GSG and GPG, respectively) increased α-helix and β-sheet content, leading to a smoother surface and more stable, organized gluten structure. The higher surface hydrophobicity in GLPg resulted in fewer hydrogen bonds in gluten. Low-Field NMR revealed that GLPg promoted uniform water distribution in GPG by increasing half-bound water content and shortening relaxation times. By leveraging the distinct structural properties of natural *Ganoderma lucidum* polysaccharides and proteoglycans, this research gives a comparison of these two natural hydrocolloids and finds GLPg with higher surface hydrophobicity optimizes gluten structure with a stable and stronger network. Our findings offer mechanistic insights into the interactions between fungal hydrocolloids and gluten, providing a scientific foundation for utilizing natural *Ganoderma lucidum* for innovative functional wheat products.

1. Introduction

Ganoderma lucidum is a traditional Chinese medicinal and edible fungus with bioactive components that include polysaccharides, triterpenes, and ganoderic acids. Due to its high bioactivity, such as antioxidant and anti-inflammation properties, *Ganoderma lucidum* is widely used in nutraceutical foods (González-Díaz et al., 2024). In addition, *Ganoderma lucidum* can enhance food texture because of its high polysaccharide content (Bao et al., 2025). Previous studies showed that liquid fermented *Ganoderma lucidum* broth enhanced dough quality and illustrated the role of crude *Ganoderma lucidum* proteoglycan in this improvement (Xu et al., 2024, 2025). Liquid fermentation offers more consistent quality, a shorter cultivation period, and controllable conditions, enabling reproducible operation and showing great potential for application in the food industry. Wheat is used in many food products such as bread, pasta, noodles, and pastries. The success of wheat in various applications largely depends on gluten formation, which provides the distinct chemical and physical characteristics of wheat dough (Wieser et al., 2022; Zhou et al., 2021). Adding flour improvers is a common practice for wheat products such as bread. Additives such as

* Corresponding authorSchool of Food Science and Technology, Jiangnan University, 1800 Lihu Road, Wuxi, 214122, PR China.
** Corresponding author.
E-mail addresses: 18115392285@163.com (J. Luan), xmxu@jiangnan.edu.cn (X. Xu).

https://doi.org/10.1016/j.foodhyd.2025.111840
Received 27 May 2025; Received in revised form 7 July 2025; Accepted 1 August 2025
Available online 5 August 2025

oxidizing agents, emulsifiers, enzymes, and hydrocolloids help improve the dough's characteristics and final product quality (Ferrero, 2017). Optimal gluten properties allow the incorporation of nutrient-rich components, such as whole grains, fibers, or plant-based proteins, which are often restricted by poor dough performance, thereby supporting the formulation of healthier cereal-based products. Therefore, for scientists and food producers, a thorough understanding of how to improve the qualities of gluten is essential since this can promote the development of healthier, more nutrient-dense, and ecologically friendly solutions (Zhang, Ruobing, et al., 2023).

Hydrocolloids, which are widely used as thickeners and gel formation in the food industry, mainly affect the characteristics of gluten protein through electrostatic interactions and hydrogen bonds (Zhang, Liu, et al., 2023). Both covalent bonds and non-covalent bonds, including hydrogen bonds, hydrophobic interactions, and electrostatic interactions, may affect the structure of the gluten network. Among these, hydrophobic interactions are the most prevalent during dough development (Iwaki et al., 2023). Exogenous compounds hydrophobic or hydrophilic functional groups can significantly influence this process. A previous study demonstrated that anionic hydrocolloids, such as carrageenan isoforms and pectin, can interact with gluten proteins, forming produce a soluble hydrocolloid-gluten complexes with hydrophilic properties (Ribotta et al., 2005). Understanding how these exogenous hydrophilic and hydrophobic groups affect gluten hydration and disulfide bond bridging in gluten formation offers valuable insights into the molecular mechanisms of gluten network development and presents new opportunities for improving dough functionality and final product quality. During gluten formation, SS bonds between the high molecular weight glutenin subunits (HMS), along with the SS bonds and non-covalent bonds such as van der Waals forces, hydrogen bonds and hydrophobic interactions, among the low molecular weight glutenin subunits (LMS), the monomeric gliadin and HMS, collectively support the stable network in gluten dough (Wang et al., 2015). *Ganoderma lucidum*-derived polysaccharides have shown encouraging possibilities in raising the functional properties of dough but their structure and the influence of different bioprocesses on the quality require further research (Xu et al., 2025). Our study focused on two kinds of hydrocolloids: proteoglycans from liquid fermented *Ganoderma lucidum* and polysaccharides from *Ganoderma lucidum* fruiting bodies, and compared their effect on the quality of dough in relation to gluten.

2. Chemicals and methods

2.1. Chemicals

Gluten flour was purchased from Wuxi Minlong Food Co., Ltd (Wuxi, China). Maize flour was bought at the local market. Potato dextrose agar (PDA) and potato dextrose broth (PDB) were purchased from Sinopharm Chemical Reagent Co., Ltd (Shanghai, China). Other chemicals were purchased from Sigma-Aldrich (St. Louis, MO, USA). *Ganoderma lucidum* was preserved at 4 °C.

2.2. Extraction of GLPs and GLPg

GLPs and GLPg were extracted and purified from *Ganoderma lucidum* fruiting bodies and fermented *Ganoderma lucidum*, respectively. Generally, the procedure from a prior study was followed in the manufacture of the liquid fermented *Ganoderma lucidum* broth and the extraction of crude GLPg (Xu et al., 2025). The crude GLPs was prepared by extracting the soluble parts from *Ganoderma lucidum* powder (10 g) with hot water (500 mL, 60 °C) for further extraction. Three times alcohol was added to the solution and used to clear the dark precipitate to extract the crude GLPs. After that, the crude GLPs was freeze-dried for further purification. Following the removal of the free protein using the Sevage reagent (25 % chloroform-butanol (v/v)), the crude GLPs and GLPg were each dissolved in water (1 mg/mL) and subsequently separated by HiPrep DEAE FF 16/10 column (Cytiva, Marlborough, MA, USA.). A solution of NaCl (0.2–1.2 M) was subsequently eluted at a flow rate of 0.5 mL/min. The elution process was monitored by a UV detector at 280 nm and each tube (3 mL/tube) was collected meanwhile and analyzed by the phenol-sulfuric acid method at 490 nm (Fig. S1) (Huang et al., 2011). A proteoglycan solution of 0.4 M and polysaccharide solution of 0.2 M was collected and purified by Superdex™ 75 10/300 GL (Cytiva, Marlborough, MA, USA.) at a flow rate of 0.5 mL/min.

2.3. Characteristics of GLPs and GLPg

2.3.1. The structure analysis of GLPs and GLPg

The structure and functional groups of GLPs and GLPg were analyzed by flourier transform infrared spectroscopy (FTIR, Antaris II, Thermo Fisher Scientific Inc., USA) and circular dichroism (CD). Anhydrous potassium bromide was combined with powders (5 mg) at a ratio of 1:200 before being pressed into slices for FTIR analysis. The spectrum ranged from 400 to 4000 cm^{-1} and the data was analyzed by OMNIC 8.0 software (Thermo Nicolet Corp., USA). For CD analysis, solutions containing 1 mg/mL GLPs or GLPg were analyzed at a range of 190–300 cm^{-1}. The CD data were analyzed using the pro-Data viewer program (Applied Photophysics, USA).

2.3.2. The composition of GLPs and GLPg

The content of several monosaccharides (GaiA, Rha, Rib, Xyl, GlcA, Man, Ara, Gal, and Glc) and amino acids (Asp, Tyr, Glu, Val, Ser, Met, His, Phe, Gly, Ile, Thr, Leu, Arg, Lys, Ala, and Pro) was examined using high-performance liquid chromatography (HPLC, Agilent 1100, Agilent Technologies, Inc., CA, USA) to determine the composition of GLPs and GLPg.

2.3.2.1. The analysis of amino acids. For the determination of amino acids content, GLPs and GLPg powders were dissolved in water (10 mg/mL). Subsequently, 8 mL 6 M HCl was added to the solutions, followed by thorough mixing. Then, samples were evaporated using Termovap Sample Concentrator for 3 min and subjected to hydrolysis at 120 °C for 24h. All solutions were added to 4.8 mL 10 M NaOH and brought to 25 mL with distilled water. Samples were centrifuged at 10000 rpm for 10 min and then filtered by 0.22 μm filter before being analyzed by HPLC, equipped with an ODS Hypersil column (5 μm, 4.0 mm × 250 mm).

2.3.2.2. The analysis of monosaccharides. PMP pre-column derivatization method was used to analyze monosaccharides compositions following the method from Wang et al. (2023) with slight modifications. GLPs and GLPg (10 mg) were hydrolyzed with TFA (4 mL, 2 M) at 110 °C for 4h. After hydrolysis, the TFA was removed by nitrogen flow, and the remaining sample was dissolved in 1 mL distilled water, with the process repeated three times. The hydrolyzed samples were then treated with 0.6 mL NaOH (0.3M) and 3 mL PMP (0.5M), followed by incubation at 70 °C for 1 h. Then, the solutions were neutralized by HCl (0.3M) and extracted three times with an equal volume of chloroform. The aqueous phase was filtered and analyzed by HPLC using an Agilent C18 column (Agilent, CA, USA). The mobile phase consisted of phosphate buffer saline and acetonitrile (82:18, v/v), with a flow rate of 1 mL/min. The DAD detector was set at 245 nm, and the column temperature was maintained at 30 °C.

2.3.3. Determination of surface hydrophobicity

Surface hydrophobicity was determined using the ANS fluorescence method described by Zhou et al. (2023) with slight modifications. In brief, GLPs and GLPg were diluted (0.1–1 mg/mL) in a 100 mM sodium phosphate buffer (pH 6.8). Then, the prepared solutions (4 mL) were mixed with 20 μL ANS agent (8 mM, 100 mM sodium phosphate buffer, pH 6.8). After the reaction in the dark for 15 min, fluorescence intensity was measured using a Cary Eclipse Fluorescence Spectrometer (Agilent,

USA). The excitation wavelength was set at 390 nm and the emission wavelength was set at 470 nm. The surface hydrophobicity was quantified as the slope of the emission intensity at different concentrations.

2.3.4. The thermal properties and crystallinity of GLPs and GLPg

Thermogravimetric analysis (TGA) was carried out using a TGA2 (Mettler–Toledo, Schwerzenbach, Switzerland) to monitoe the degradation of samples during increasing temperature. Sample was heated at 10 °C/min from 50 °C to 600 °C and the weight loss was recorded. X-ray diffraction was used to determine the crystallinity of samples. The spectrum ranging from 5 to 40° was collected by D2 PHASER (Bruker AXS GmbH, Karlsruhe, Germany). The scanning speed was set as 5°/min, with a current of 15 mA and voltage of 30 kV, under the radiation of CuKα.

2.3.5. The morphology of GLPs and GLPg

The morphology of GLPs and GLPg was analyzed by scanning electron microscopy (SEM) (SU1510, Hitachi, Japan). The powder of GLPs and GLPg was affixed to the holder and coated with a 50 mm gold layer to enhance conductivity. The analysis was conducted at an accelerating voltage of 3 kV.

2.3.6. Average size and zeta potential analysis

GLPs and GLPg (1 mg/mL) were analyzed for particle size distribution and zeta potential in the aqueous solution using a Malvern Zetasizer Nano ZS (Malvern Instruments, Worcestershire, UK). The average particle size and zeta potential value for each sample were recorded.

2.4. Gluten dough preparation

Gluten dough was prepared using gluten flour and water. Specifically, GLPs or GLPg powder was thoroughly mixed with gluten flour (moisture content: 4.1 %). Distilled water (50 %, w/w) was then added to the mixture, and the components were stirred at a controlled temperature for 5 min at 63 rpm using a Farinograph (Brabender, Duisburg, Germany) to obtain GLPs-incorporated gluten dough (GSG) and GLPg-incorporated gluten dough (GPG).

2.5. Characteristics of gluten dough

2.5.1. The morphology of gluten dough

The gluten dough was freeze-dried and cut into small pieces for SEM analysis. Other steps followed the method from section 2.3.5. The preparation for atomic force microscope (AFM) analysis was conducted as follows. Briefly, freeze-dried samples (1 mg) were dissolved in 0.5 M acetic acid solution and thoroughly mixed. The mixture was then centrifuged at 4700 g for 10 min, and the supernatant was collected for analysis. The clarified solution (10 μL) was deposited onto a cleaved mica substrate and then dried under a stream of clean air. AFM imaging was performed using a Nanoscope AFM (Bruker, Billerica, MA, USA), with a sample stage size of 10 μm × 10 μm. Image analysis was conducted using Nanoscope Analysis (Bruker, Billerica, MA, USA).

2.5.2. The zeta potential of gluten dough

The freeze-dried gluten dough was ground into powder and subsequently dispersed in distilled water to prepare a 1 mg/mL gluten suspension (Wang et al., 2021). The zeta potential of the solution was then measured after centrifuging, following the procedure described in section 2.3.6.

2.5.3. The structure analysis

The analysis of Raman spectroscopy is carried out with following method. The powders of GSG and GPG were placed on a microscopy slide covered with tin foil and analyzed using a laser at 532 nm (HORIBA Jobin Yvon S.A.S., Palaiseau, France). Additionally, gluten dough was ground into flour and its second structure was examined following the FTIR method as described in section 2.3.1.

2.5.4. The rheological properties

The rheological properties of GSG and GPG were measured using a DISCOVERY HR-3 rheometer (TA instrument Inc., New Castle, USA) with a 20 mm parallel plate. Gluten dough was placed on a parallel plate and the temperature was set at 25 °C (loading gap: 20 mm). The strain was chosen from the linear viscosity curve of G′ and G″ and the values of G′, G″ and tanδ were collected with frequencies from 0.1 to 10 Hz.

2.5.5. Gluten solubility in different solvents

The interactions in gluten were measured using the method from Wang et al. (2017, 2018). Protein solubility in different solvents was analyzed to assess various chemical interactions. Generally, gluten flour (100 mg) was dissolved in 10 mL of different solution buffers, respectively. These buffers to dissolve protein were prepared by phosphate-buffered saline (PBS, 0.5 M, pH 7.0): 0.6 M NaCl in PBS (SA), 0.6 M NaCl and 1.5 M urea in PBS(SB) and 0.6 M NaCl and 8 M urea in PBS(SC). After extraction for 1 h at room temperature (RT, 25 °C), mixtures were centrifuged at 4700 g for 10 min (RT). The protein content in the supernatant was assessed using a BCA Protein Assay Kit (Megazyme, XYZ123).

2.5.6. Water distribution in gluten

The water distribution was analyzed by Low-field 1H nuclear magnetic resonance (LF-NMR) (MesoMR23-060V–I; Shanghai Niumag Corporation, Shanghai, China). The spin-spin relaxation time (T_2), which could reflect the water distribution of wheat dough during storage, was recorded, as well as different proportions of different kinds of water. The sample of each group (2.5 g) was packed with preservative film to avoid water loss during the test. The pulse parameters were set with 1000 ms of interval duration, 0.4 ms of echo duration, 2 scans, and 2000 echoes.

2.6. Statistical analysis

All data are presented as mean ± standard deviation. Each experimental series included at least three replicates ($n = 3$) unless otherwise indicated. Statistical analysis was performed using one-way analysis of variance (ANOVA), and means were compared using Duncan's multiple range test with SPSS 20.0 software (SPSS Inc., Chicago, USA). A p-value of less than 0.05 was considered statistically significant.

3. Results and discussion

3.1. The characteristics of GLPs and GLPg

3.1.1. The structure analysis of GLPs and GLPg

GLPs and GLPg are the main fractions of two *Ganoderma lucidum*-derived products. One was directly extracted from *Ganoderma lucidum* fruiting bodies and the other from liquid-fermented *Ganoderma lucidum*. The molecular structure of GLPs and GLPg were initially analyzed by FTIR to characterize the composition of functional groups. As shown in Fig. 1, FTIR spectrums of GLPs and GLPg from 400 to 4000 cm^{-1} were collected. The absorption bands at approximately 3420, 2920 1385, and 1650 cm^{-1} (indicated by dashed lines) were attributed to the stretching vibrations of the O-H, C-H bonds, as well as the asymmetric vibration stretching of the C=O group in the carboxyl functional group of the monosaccharide units within the polysaccharide chains (Ahmadi et al., 2022; Chen et al., 2022; Hong et al., 2021; Shao et al., 2024). The positions and intensities of these peaks provide insight into the potential characteristics of polysaccharides in GLPs and GLPg.

The comparison of GLPs and GLPg based on detailed bands from FTIR analysis is presented in Table 1. Specific bands in the fingerprint region (1000-1200 cm^{-1}) were used to identify the anomeric carbon configurations, which could generally be concluded as different carbon configurations (α or β) and varying sugar rings (furanose or pyranose)

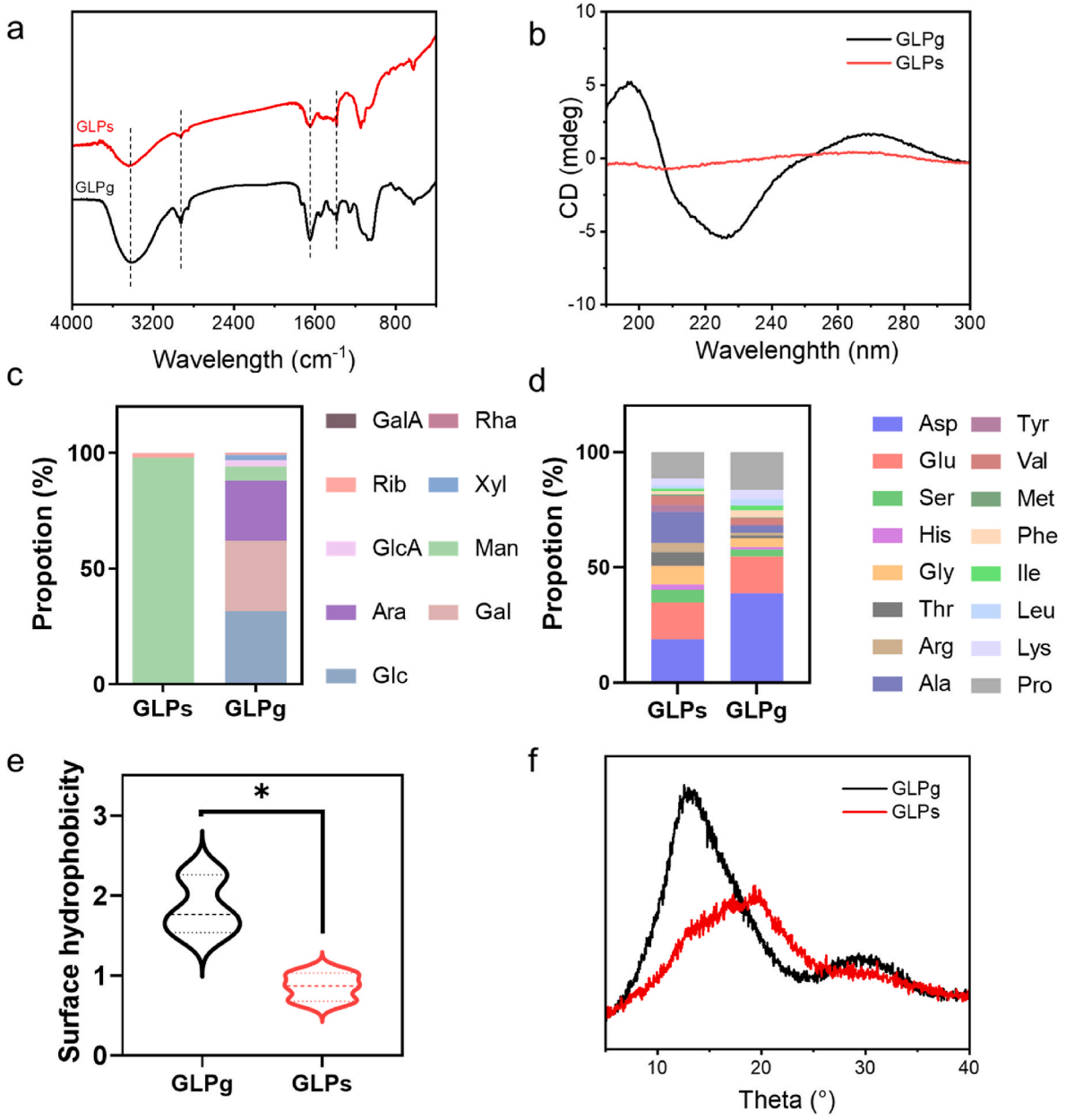

Fig. 1. The (**a**) FTIR spectra from 400 to 4000 cm^{-1} and (**b**) CD spectra in the 190–300 nm range of GLPs and GLPg. The dashed line in Fig. 1a demarcates the absorption bands at approximately 3420, 2920, 1385, and 1650 cm^{-1} GLPs and GLPg. The (**c**) monosaccharide composition and (**d**) amino composition of GLPs and GLPg. (**e**) The surface hydrophobicity of GLPs and GLPg. (**f**) XRD results for GLPs and GLPg.

(Guo et al., 2018; Hong et al., 2021). Three absorption peaks within the wavelength range of 1000–1200 cm^{-1} indicated the presence of pyranose forms in both GLPg (1044 (w), 1072 (w) and 1116 (sh) cm^{-1}) and GLPs (1065 (sh), 1115 (m) and 1146 (s) cm^{-1}) (Hong et al., 2021).

Furthermore, the bands at 1543 (s) and 1259 (vs) cm^{-1} in the spectrum of GLPg were characteristic of N-H/C-H bonds in proteins, along with a weak symmetrical stretching region from 1320 to 1450 cm^{-1}, indicating the presence of carboxyl groups (1384 (vs) and 1410 (w) cm^{-1}. These peaks were notably weak in GLPs, however (Bhaumik et al., 2020). Additionally, peaks at 1647 (vs) and 1543 (sh) cm^{-1} were identified as amid stretching bands from proteins (Chylinska et al., 2016). The presence of these signals, originating from protein, further supported the identification of GLPg from fermented *Ganoderma lucidum* broth as a proteoglycan.

CD is a method widely used to detect the aromatic amino acid residues in proteins, as well as disulfide bonds, which exhibit characteristic absorption bands in the near-ultraviolet region (250–320 nm) and provide insights into the conformational state in carbohydrates, such as polysaccharides chains, due to the significance of chirality as a key feature in their structure (Chen et al., 2022; De et al., 2020). In far UV-CD regions, the amide chromophore of the peptide bond in proteins dominates, as it exhibits different absorption to left and right polarized light (Pelton & McLean, 2000). Previous reports have shown that the diverse structure of polysaccharides, such as disordered chains, extended rigid chains, or collapsed flexible and helix-like chains, resulted in a complex CD spectrum (De et al., 2020; Lopez-Torrez et al., 2015). The spectrum of the GLPs and GLPg in the range of 190–300 nm is shown in Fig. 1b. There was a distinct ellipticity of GLPg observed in the CD spectrum, while that of GLPs was much weaker. GLPg exhibited a minimum ellipticity at 225 nm and a maximum at 198 nm. Lopez-Torrez et al. (2015) proved that the decrease of ellipticity below 195 nm was attributed to the substitution of the polypeptide backbone with

Table 1
Characterizations of GLPs and GLPg in detailed bands from FTIR spectra.

Assignment	Wavelength/cm^{-1} (intensity)		Main contribution
	GLPg	GLPs	
Ring vibration	800 (m)	803 (m)	The symmetrical stretching vibrations of α-pyran; MANB
C1–H bending	873 (w)	870(s)	Polysaccharide
C–C stretching ring	1044 (w)	–	Pyranose forms
C–O stretching, C–C stretching	–	1065 (sh)	Pyranose forms
C–C stretching ring	1072 (w)	–	Pyranose forms; Galactan
stretching vibrations of the pyranose C-O-C bonds	1116 (sh)	1115 (m)	Pyranose forms
Vibrations O–C–O	–	1146 (s)	Pyranose forms; glycosidic bond
C-H	1259 (vs)	–	Protein
C–H bending	1384 (vs)	1384 (vs)	Carboxyl groups
the stretching vibrations of C-H bonds	1410 (w)	1416 (w)	Monosaccharide units; carboxyl groups
asymmetric stretching modes vibration of methyl esters	1448 (sh)	–	Methyl esterification
Amid II N–H deformation	1543 (s)	–	Protein
amid stretching bands	1647 (vs)	–	Protein

w: weak, m: medium, s: strong, vs: very strong, sh: shoulder.

polysaccharide chains, a phenomenon also observed in GLPg. Moreover, a positive band near 195 nm and a negative band near 225 nm showed a β-structure in GLPg, which also illustrated the presence of protein structure inside (Pelton & McLean, 2000). Therefore, certainly GLPg was partially structured with both polysaccharides and peptides, which was consistent with the structure analysis obtained by FTIR.

3.1.2. The composition of GLPs and GLPg

In this section, the composition of GLPs and GLPg was analyzed to further explore their difference in depth, focusing on the monosaccharide and amino acid composition. The monosaccharide composition and amino composition of GLPs and GLPg are shown in Fig. 1c and d. The main monosaccharide in GLPs was Man and the top three monosaccharides that constituted GLPg were Glc, Gal, and Ara, respectively (Fig. S2). The amino acid contents in GLPs and GLPg were 9.65 % and 28.67 %, respectively. It can be concluded that GLPg is a kind of proteoglycan, primarily composed of peptides and galactoglucan, while GLPs is a form of heteromannans with a small amount of peptides (Faustino et al., 2021). Furthermore, the FTIR bands of GLPs at 1065 (sh) cm^{-1} and the specific bands, 870 (s) and 803 (m) cm^{-1}, which could be attributed to the mannose in mannan, support this conclusion (Liu et al., 2021). In both GLPs and GLPg, the top three amino acids were Asp, Glu, and Pro with proportions of 18.9 %, 15.8 %, and 11.5 % in GLPs, and 38.8 %, 16.0 %, and 16.4 % in GLPg, respectively. While both GLPs and GLPg shared the same top three amino acids, they differed in their total contents. The side chains of these amino acids, influenced by their local environment, contributed to the overall hydrophilicity and hydrophobicity of protein, thereby forming the hydrophobic core region of the protein (Banach et al., 2020; Di Rienzo et al., 2021). These amino acid residues contribute to the higher hydrophobicity of GLPg, enhancing its overall hydrophobic character (Bonella et al., 2014).

3.1.3. The physical properties of GLPg and GLPs

In this section, the thermal properties, crystallinity, surface hydrophobicity, DLS, and zeta potential of GLPs and GLPg were analyzed to gain a comprehensive understanding of their physical characteristics and provide essential insights into how they interact with gluten.

A higher zeta potential resulting from stronger electrostatic repulsion between molecules, contributes to improved stability. In contrast, a lower zeta potential suggests a reduced repulsive force, which may led to macromolecules aggregation, where attractive van der Waals forces become dominant (Joseph & Singhvi, 2019). Therefore, zeta potential can provide valuable insights into the presence of charged functional groups and the nature of intermolecular interactions in macromolecular systems. The surface hydrophobicity of GLPs and GLPg was compared regarding the composition of functional groups. The surface hydrophobicity of GLPg was significantly higher than GLPs, which can be attributed to the peptide component in the proteoglycan structure (Fig. 1e) (Bonella et al., 2014). For amphiphilic macromolecules, increased hydrophilic conjugation can stabilize a larger surface area, leading to the formation of smaller particles, which is corresponded to previous report (Yin et al., 2017).

The XRD pictures of GLPs and GLPg are shown in Fig. 1f. The crystalline curve exhibited a typical "bun-shaped" bend, which was regarded as characteristic of amorphous polysaccharides (Qian et al., 2009). As shown in Fig. 2, the DLS of GLPs and GLPg were 165.6 and 381.78 nm, respectively, and the zeta potentials of GLPs and GLPg were −1.35 and −6.4 mV, respectively. GLPs is an anionic polysaccharide, while GLPg is an anionic proteoglycan. The higher absolute value of the zeta potential in GLPg showed a greater system stability compared to GLPs. The difference can be attributed to the different amino acid and monosaccharide compositions (Huang et al., 2018; Wang et al., 2022).

The thermal properties of GLPs and GLPg were analyzed using TGA. The two samples exhibited distinct behaviors when heated to 600 °C (Fig. S3). The TG and DTA curves showed the change in weight of GLPs and GLPg with the increase of temperature and the rate of mass change, respectively. The weight loss below 200 °C was attributed to the removal of moisture left from polysaccharides (Liu, Yu, et al., 2022). The main mass loss in GLPs and GLPg appeared at 100–250 °C and 200–350 °C, respectively. The maximum mass loss rate occurred at 284 °C, where 33.4 % of the GLPg mass was lost. In GLPs, the maximum mass loss rate occurred at 193 °C, and was less than the maximum loss rate of GLPg. The breakdown of peptide linkages into small molecular fragments at high temperatures may explain the weight loss observed in GLPg around 284 °C (Jin et al., 2024).

3.1.4. The morphology of GLPs and GLPg

Polysaccharides differ in their microstructure due to their overall complicated structure (Liu, Hu, et al., 2022). As shown in Fig. 2c and d, GLPs and GLPg both had an amorphous structure. Under SEM with larger magnification, the surface of GLPs seemed smoother than GLPg (Fig. 2e and f). Different structures and origins of GLPs and GLPg resulted in differences in size, shape, and surface morphology (Liu, Hu, et al., 2022).

3.2. Comparison between different gluten doughs

3.2.1. Comparison in surface morphology

The surface morphology of gluten dough was analyzed by SEM (Fig. 3a–f). At 300x magnification (scale bar: 100 μm), gluten doughs were porous, and the gluten dough of GLPs had a denser structure than that of the control and GLPg. At 4500x magnification (scale bar: 10 μm), the finer structures of gluten dough were shown. Moreover, the gluten doughs of GLPs and GLPg were visibly smoother than the control. Multiple and uniform apertures provided GLPg-treated gluten dough with a stronger structure to hold more gas during fermentation (Li et al., 2023). The smoother surface can be attributed to the strong hydrophilicity, forming colloidal shapes with high viscosity after water absorption (Xiong et al., 2024).

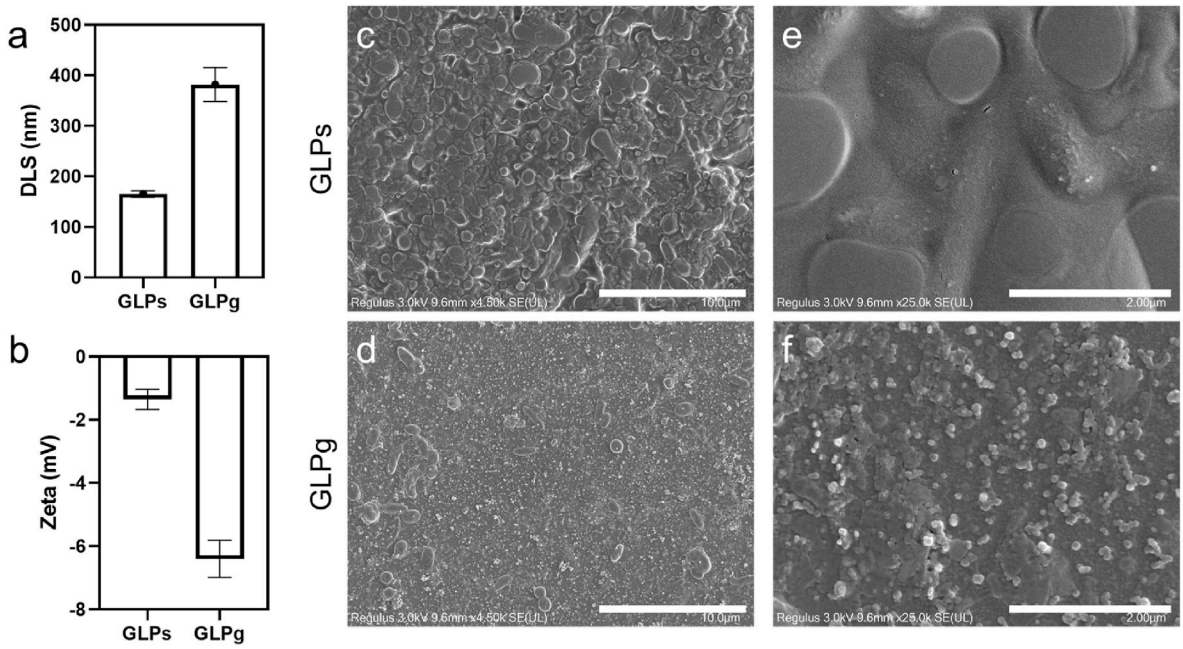

Fig. 2. The size (**a**) and zeta potential (**b**) of GLPs and GLPg (10 mg/mL) analyzed by dynamic light scattering (DLS). SEM images for GLPs (**c** and **e**) and GLPg (**d** and **f**). Scale bars for **c** and **e**: 10 μm; scale bars for **d** and **f**: 2 μm. Data are presented as mean ± s. d. ($n = 3$).

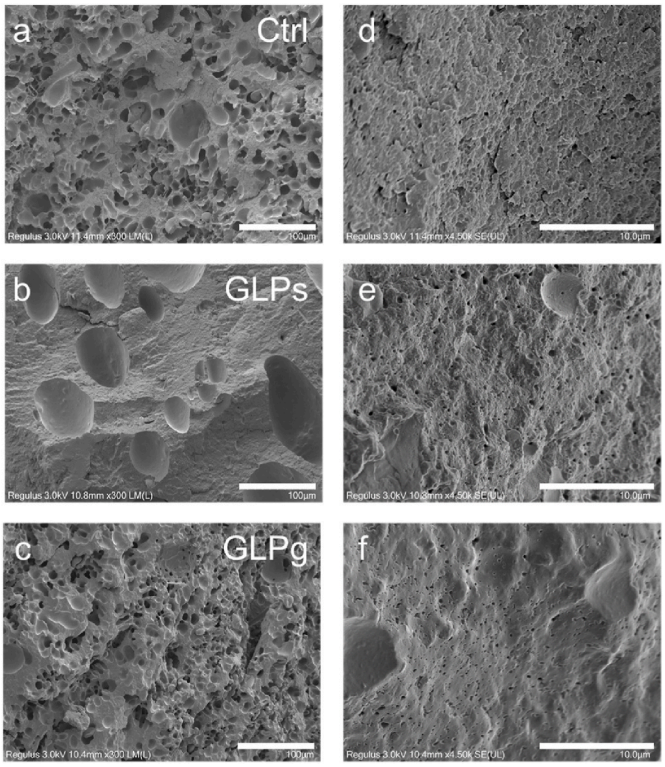

Fig. 3. The SEM pictures of **a** and **d** gluten dough without any treatment, **b** and **e** gluten dough added with GLPs, and **c** and **f** gluten dough added with GLPg. Scale bars for **a-c**: 100 μm; scale bars for **d-e**: 10 μm.

3.2.2. Changes in zeta potential

As a key indicator to determine the attractive and repulsive forces among large moleculars in solution, the zeta potential of each sample was also recorded to illustrate the difference between GSG and GPG (Wang et al., 2022). After adding electronegative GSG and GPG, the zeta potential increased to 9.53 and 10.4 mV from 5.57 mV, respectively, which showed higher stability in GPG (Fig. S4). The higher interaction between proteins and GLPg might help to explain this result. GLPg with a higher negative charge on the surface can attract positively charged protein molecules and produce electrostatic interactions to form hydrophilic complexes (Zhang, Liu, et al., 2023).

3.3. Comparison in structure

The secondary structure of protein is a good way to understand the change in gluten dough texture at the molecular level (Zhou et al., 2021). The proportions of antiparallel β-sheet, β-turn, α-helix, and β-sheet are shown in Table 2. GLPs and GLPg significantly decreased the proportion of antiparallel β-sheet and β-sheet, while the proportions of α-helix and β-sheet increased in these two groups when compared with the control. The protein structure tends to be ordered with fewer antiparallel β-sheet and α-helix content, which might be attributed to the destruction of a flexible structure by the addition of GLPs and GLPg (Li et al., 2023). The probable explanation for this might be that hydration between hydrocolloids and gluten protein helps enhance the stable ordered structure to adapt to changes in the overall system. The GPG exhibited a greater increase in α-helix and β-sheet content compared to the GSG. GLPs and GLPg had different structures, which means different interactions with gluten protein. Fewer α-helix and β-sheet in GSG illustrated the interference of GLPs to the helical structure or the loose and dispersed binding between GLPs and protein, which was in line with the lower surface hydrophobic ability of GLPs.

Table 2
The second structure of gluten dough with different treatments was analyzed by FTIR.

	Ctrl	GSG	GPG
antiparallel β-sheet	54.01 ± 0.07a	53.6 ± 0.18b	53.42 ± 0.14b
β-turn	32.61 ± 0.1a	31.64 ± 0.68b	30.96 ± 0.78b
α-helix	9.07 ± 0.1c	9.74 ± 0.28b	10.1 ± 0.37a
β-sheet	4.33 ± 0.11c	5.05 ± 0.34b	5.54 ± 0.52a

Data are presented as mean ± s. d. ($n = 3$). Different lowercase letters indicated the significant difference of antiparallel β-sheet, β-turn, α-helix, and β-sheet in different gluten dough of Ctrl, GSG, and GPG ($p < 0.05$).

The aggregation and morphology of gluten are shown in Fig. 4. The 3D peak force and roughness (Rq) provide important information when analysing the cross-linking aggregation of gluten protein. Here, it was obvious that the gluten proteins aggregated granularly. Rq of Ctrl was higher than GSG and GPG, showing the roughest surface among each group with more microscopic pores, protrusions, or grooves present, like the SEM in section 3.2.1. In GSG and GPG, the aggregation of protein and hydrocolloids led to a uniform surface, which was changed by the interaction between gluten and GLPs or GLPg.

3.4. Rheological properties

Fig. 5a and b shows the change in G′ and G″ with the addition of GLPs and GLPg at different frequencies. Generally, G′ is higher than G″, illustrating the stronger and lower extensity of gluten dough with higher elasticity (Li et al., 2019). The presence of GLPg on gluten formed a network with better elasticity and a more compact and stable structure, notably exhibited in a poriferous and smoother structure, as indicated by the higher G′ observed in GPG. The change in tanδ was not as significant as for G' (Fig. 5c). This could be attributed to the higher surface hydrophobicity, which gave GLPg the ability to promote protein cross-linking while not affecting fluidity (Li et al., 2023). GSG had a higher tanδ while G′ did not change much, indicating the higher the relative fluidity of GSG increased. It could indicate that GLPs may be more inclined to disperse in the protein network, thereby reducing the overall stability of the network and making the system show higher mobility.

3.5. Interactions between different gluten doughs

The formation of S-S presented as intrachain disulfide bonds within a protein and interchain disulfide bonds between proteins is important to the structure and function of gluten (Nawrocka et al., 2016). Raman provided an intuitive and convenient method to get to know the changes in the disulfide bridges region (490-550 cm^{-1}) (Nawrocka et al., 2017). As shown in Fig. 6a, the proportion of SSt-g-g and SSt-g-t in GLPs and GLPg groups significantly decreased, and the proportion of SSg-g-g significantly increased in GLPs and GLPg. There was no significant difference between GLPs and GLPg. In GPG and GSG, the addition of GLPg and GLPs prevented the conversion of disulfide bonds from the most energetically stable (g-g-g) conformation to less energetically stable

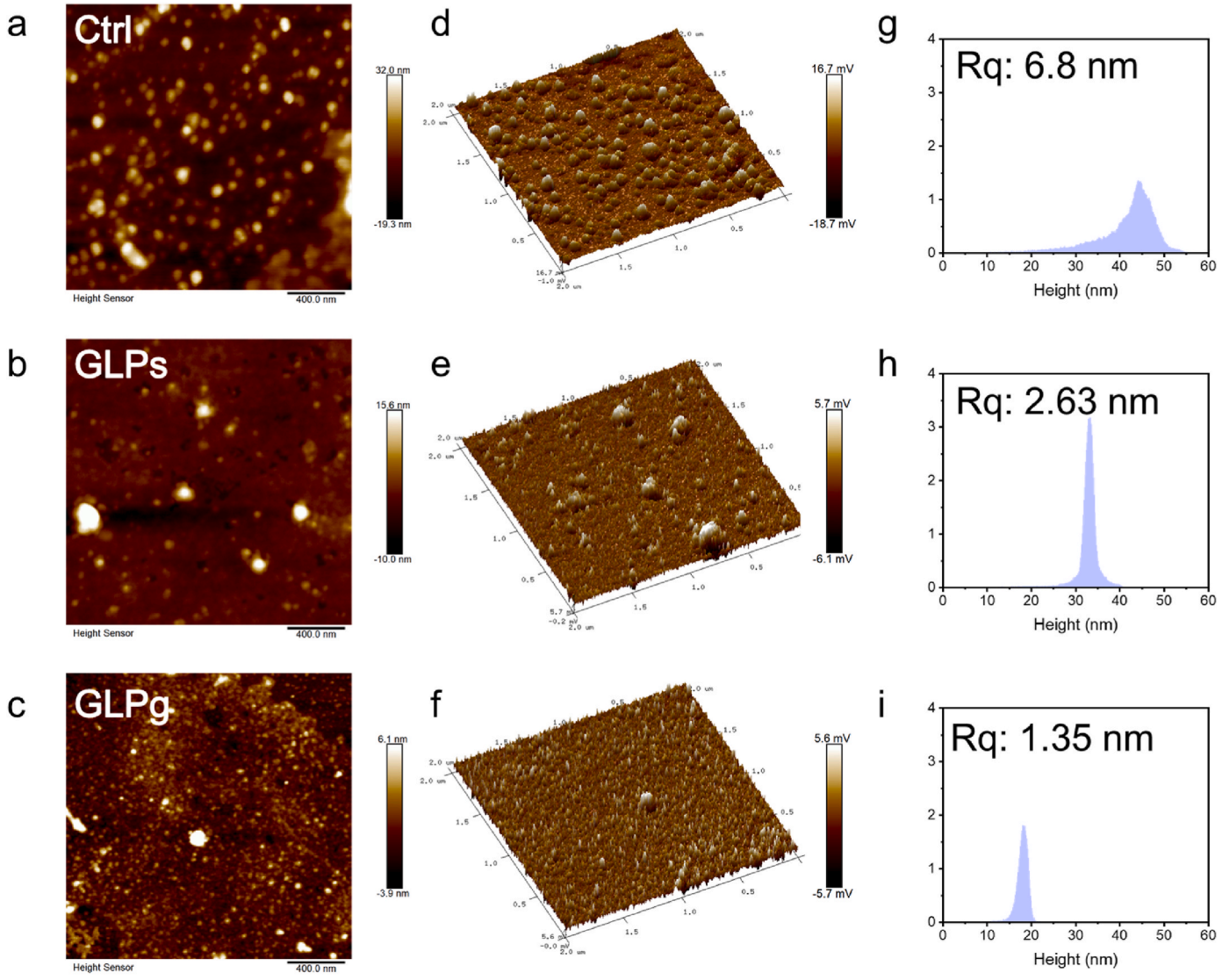

Fig. 4. AFM topography of gluten proteins with different treatments (**a**: gluten proteins without any treatment; **b**: gluten proteins added with GLPs; **c**: gluten proteins added with GLPg). The 3D peak force images of gluten proteins with different treatments (**d**: gluten proteins without any treatment; **e**: gluten proteins added with GLPs; **f**: gluten proteins added with GLPg). Depth histogram of gluten proteins with different treatments (**g**: gluten proteins without any treatment; **h**: gluten proteins added with GLPs gluten proteins added with GLPg; **i**: gluten proteins added with GLPg). Scale bars: 400 nm.

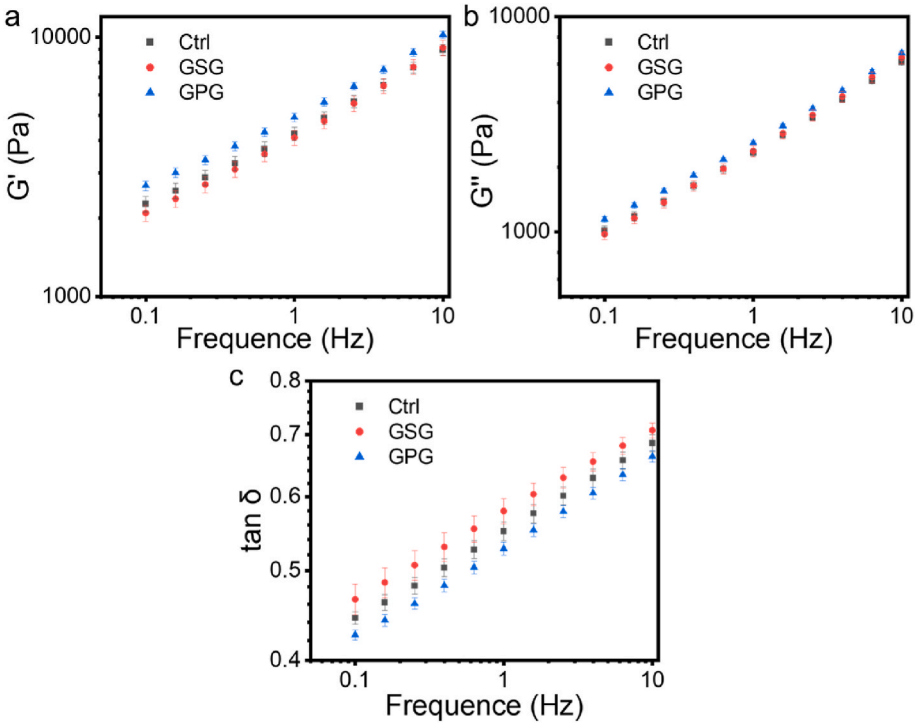

Fig. 5. Changes in **(a)** storage modulus (G′), **(b)** loss modulus, and **(c)** tanδ of different groups (Ctrl, GSG, and GPG).

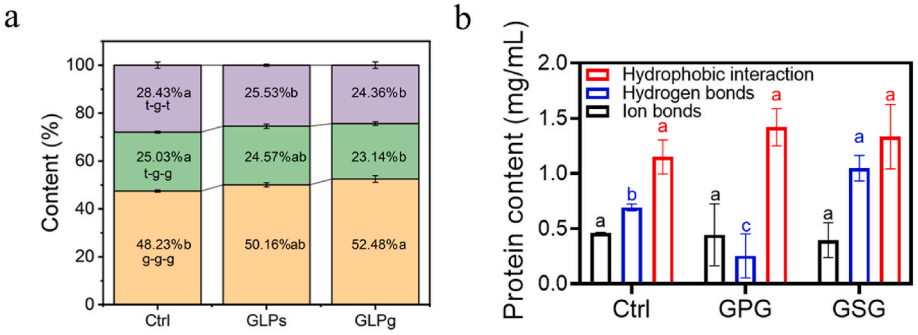

Fig. 6. **(a)** Different content of t-g-t, t-g-g, and g-g-g, constituted by the disulfide bond, in gluten with different treatments, analyzed by Raman. Data are presented as mean ± s. d. (n = 3). Different lowercase letters indicated the significant difference in content of t-g-t, t-g-g, and g-g-g in different gluten dough of Ctrl, GLPs, and GLPg. **(b)** Hydrophobic interaction, hydrogen bonds, and Ion bonds content in gluten with different treatments. Different lowercase letters with different colors indicate a significant difference among each group ($p < 0.05$).

conformations (t-g-g and t-g-t) by changing the amino acid microenvironment with an ordered structure (Krekora & Nawrocka, 2024).

During the formation of gluten structures, hydrogen bonds, ion bonds, and hydrophobic interactions all contribute to the interactions between the components, and proteoglycan and polysaccharides would interfere with this progress because of the hydrophilic and hydrophobic groups on the surface (Su et al., 2024; Zhang, Liu, et al., 2023). Therefore, understanding the chemical interactions in gluten formation helps us gain fundamental knowledge of what roles the proteoglycan and polysaccharides play in the formation of gluten and what the difference between them is. Different chemical interactions were presented by protein solubility in different solvents (Wang et al., 2018). As shown in Fig. 6b, there were no significant differences in ion bonds or hydrophobic interactions among Ctrl, GSG, and GPG. Even though GLPg had a higher surface hydrophobicity than GLPs (section 3.1.3), it could be attributed to the limited hydrophobic area when interacting with gluten protein. However, a significant decrease in hydrogen bonds was observed in GPG when compared with the Ctrl and GSG. The same tendency was found in dough with added proteoglycan in our previous study (Xu et al., 2025). GLPg had a higher surface hydrophobicity, which led to a tight combination with gluten as compared to GLPs. This might affect the degree of freedom of polar groups on the protein surface and thus decrease the number of hydrogen bonds with a softened gluten structure (Kuang et al., 2023).

3.6. *Water distribution*

GLPg gathers more water from gluten than the Ctrl, as there is a higher intermediate water content in GPG, while these interactions are stronger than those between water and gluten protein for the lower proton transverse relaxation times in GPG (Table 3). Even though there was no significant difference in the proportion of water, the higher proton transverse relaxation times for bound water in GPG than GLG were found, showing the loose interaction between water and gluten. The lower number of hydrogen bonds, along with a decrease in the water-holding ability, would lead to more free water, aligning with the

Table 3
The water distribution of different proton transverse relaxation times (T2) and water proportion (A2) of gluten dough with different treatments (Ctrl, GLPs and GLPg) in different time.

	Ctrl	GLPs	GLPg
T_{21}	0.41 ± 0.01b	0.42 ± 0.01b	0.47 ± 0.02a
T_{22}	8.41 ± 0.00a	8.41 ± 0.00a	8.41 ± 0.00a
T_{23}	1647.21 ± 342.87a	935.06 ± 160.7b	846.41 ± 96.48b
A_{21}	16.81 ± 0.18a	16.26 ± 0.27 ab	15.91 ± 0.51b
A_{22}	83.17 ± 0.19b	83.72 ± 0.27 ab	84.07 ± 0.5a
A_{23}	0.02 ± 0.00a	0.02 ± 0.00a	0.02 ± 0.01a

Data are presented as mean ± s. d. ($n = 3$). Different lowercase letters indicated the significant difference among proton transverse relaxation times (T_2) and water proportion (A_2) in different gluten dough of Ctrl, GLPs and GLPg ($p < 0.05$).

observed results. On the whole, the significant difference between GPG and the Ctrl showed that GPG absorbed water from gluten and formed a water distribution with a firm connection in the gluten-half bound water-GLPg complex, resulting in a more homogeneous water distribution within this environment (Peng et al., 2017).

3.7. Discussion of the interaction mechanism

In liquid fermentation, *Ganoderma lucidum* mycelia are actively growing under controlled conditions, which promotes the production of extracellular polysaccharides and glycoproteins, including proteoglycans (Cui et al., 2007; Zhou et al., 2014). This process involves continuous biosynthesis and excretion of macromolecules through pathways such as glycosylation and peptide synthesis (Cui et al., 2024). In contrast, fruiting body development occurs over a longer timescale and involves more storage polysaccharides and structural components with relatively lower protein content. Therefore, liquid fermentation results in hydrocolloids with higher protein content and surface hydrophobicity, as seen in GLPg. This fundamental difference in molecular composition between GLPs and GLPg is expected to influence their interaction behaviors with gluten protein networks, as discussed below.

To further illustrate the potential mechanisms by which GLPs and GLPg influence gluten structure, schematic graphs were constructed (Fig. 7). These visual models depict the interaction patterns, structural changes, and potential effects on gluten protein conformation in gluten proteins. As shown in the figure, the disulfide bond serves as a cross-link in gluten structure, and the non-covalent interactions contributes to the stability of the whole structure. The secondary structure of gluten protein served as the primary framework of the gluten dough, with water uniformly distributed throughout. However, changes in the secondary structure of the protein, non-covalent interaction, and the disulfide bridge conformations would influence the final properties of gluten. These changes occurred in gluten dough after the addition of GLPs/GLPg. After the addition of GLPs and GLPg, they would gather moisture and compete for water with gluten protein (section 3.6), with more water molecular surrounding them, resulting in a loose interaction between water and gluten. As a proteoglycan, the peptide part would provide a more hydrophobic region than GLPs, which was confirmed by the higher surface hydrophobicity (section 3.1.3). The large particle size (as indicated by higher DLS values) of GLPg may increase its spatial interaction capacity with other compositions in gluten dough.

Compared with the Ctrl, GSG and GPG had a more ordered protein structure due to fewer antiparallel β-sheets and α-helix (section 3.3). This is reflected in the schematic diagram. Notably, the fewer hydrogen bonds and the larger number of α-helix and β-sheets in GPG compared to GSG, indicating that GLPs may enhance protein folding through hydrogen-bonding interactions, whereas GLPg exerts its effects primarily through hydrophobic interactions (section 3.3 and section 3.5). Additionally, the porous structure in GPG provided a stable structure with higher G′, which led to a higher elasticity in the whole system (section 3.2.1 and section 3.4). A higher hydrophobic ability made GPG

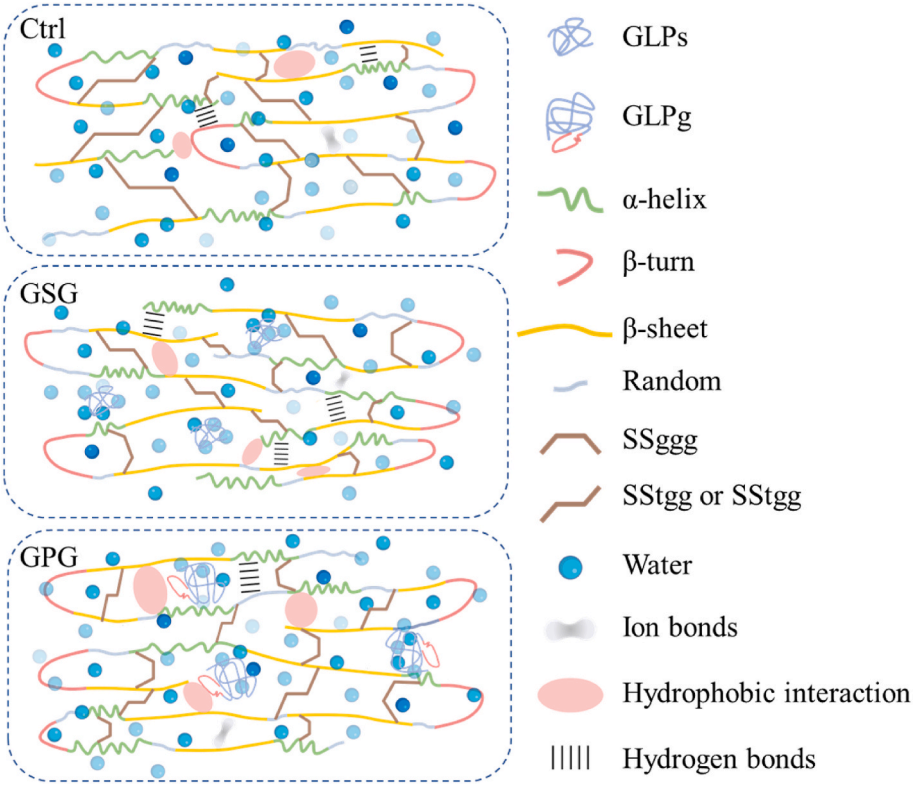

Fig. 7. Schematic representation of the proposed interaction between gluten proteins and GLPs/GLPg. Gluten without any treatment is set as the Ctrl. Created with BioRender.com.

connect more strongly to other compositions in gluten, thereby endowing the gluten dough containing GLPg with distinctive structural and functional properties.

It should be noted, however, that due to the multifactorial nature of the observed differences between GLPs and GLPg, the presentation in current schematic is based on correlation between the structural properties of hydrocolloids and final quality of gluten dough. Further studies using target model systems are needed to elucidate the specific contribution and further confirm the underlying mechanism on how hydrocolloids affect gluten formation.

4. Conclusion

This study aimed to compare the effect of *Ganoderma lucidum* polysaccharides (GLPs) and proteoglycans (GLPg) on gluten structure, based on their different compositions and structural characteristics. Both GLPs and GLPg enhanced the structural order of gluten by elevating α-helix and β-sheet content, thus stabilizing the gluten network. On one hand, GLPg, comprising polysaccharide chains and peptide components, exhibited significantly higher surface hydrophobicity than GLPs. This hydrophobicity-driven mechanism from GLPg reduced hydrogen bonds and fostered a more homogeneous environment for water distribution, proven by uniform water distribution. Moreover, GLPg enhanced elasticity and stability, forming a more compact structure, as indicated by the increased G'. These findings enhance our understanding of how hydrocolloids with different hydrophobicity impact gluten formation and interact with the key components in the dough system. Moreover, GLPg demonstrated functional advantages over GLPs and even outperformed traditional additives such as xanthan gum (Xu et al., 2025), highlighting its potential as a next-generation functional ingredient. On the other hand, from a practical standpoint, the use of GLPg produced by liquid fermentation offers a more cost-effective and resource-efficient approach than conventional extraction from fruiting bodies, supporting sustainable production. Importantly, the mechanism elucidated in this study that enhances gluten structure via hydrophobic interaction modulation, opens up novel opportunities for designing targeted dough improvers. These could be particularly valuable in clean-label baking applications, high-protein or gluten-reduced formulations, or where textural stability during storage is essential. In conclusion, this study thoroughly investigates molecular composition, especially given varying hydrophobicity, and demonstrates the different roles that GLPs and GLPg play in gluten formation. By leveraging the dual nature of GLPg and its hydrophobicity-driven effects, future functional foods, this nutraceutical compounds from *Ganoderma lucidum* not only addresses evolving consumer demands for functional foods but also improves sustainable strategies to enhance quality through optimized gluten utilization.

CRediT authorship contribution statement

Zhuojia Xu: Writing – review & editing, Writing – original draft, Investigation, Formal analysis, Data curation. **Ruth T. Ngadze:** Writing – review & editing. **Jie Shen:** Software. **Anita R. Linnemann:** Writing – review & editing. **Fengfeng Wu:** Funding acquisition. **Dan Xu:** Validation, Resources. **Jianmei Luan:** Supervision, Project administration. **Xueming Xu:** Writing – review & editing, Supervision, Funding acquisition, Conceptualization.

Declaration of competing interest

The authors declare no competing financial interest.

Acknowledgment

This work was supported by the National key research and development program of China (No. 2022YFD2100300), the National Natural Science Foundation of China (No. 32472364) and Scientific Research Project of Hebei Province (2024HBQZYCXY027).

Appendix A. Supplementary data

Supplementary data to this article can be found online at https://doi.org/10.1016/j.foodhyd.2025.111840.

Data availability

Data will be made available on request.

References

Ahmadi, S., Yu, C. X., Zaeim, D., Wu, D. M., Hu, X. X., Ye, X. Q., & Chen, S. G. (2022). Increasing RG-I content and lipase inhibitory activity of pectic polysaccharides extracted from goji berry and raspberry by high-pressure processing. *Food Hydrocolloids, 126*. https://doi.org/10.1016/j.foodhyd.2021.107477

Banach, M., Fabian, P., Stapor, K., Konieczny, L., & Roterman, A. I. (2020). Structure of the hydrophobic core determines the 3D protein structure-verification by single mutation proteins. *Biomolecules, 10*(5). https://doi.org/10.3390/biom10050767

Bao, C., Yan, M., Diao, M., Anastasiia, U., Zhang, X., & Zhang, T. (2025). Effect of Ganoderma lucidum water extract on flavor volatiles and quality characteristics of set-type yogurt. *Food Chemistry, 464*(Pt 2), Article 141687. https://doi.org/10.1016/j.foodchem.2024.141687

Bhaumik, M., Dhanarajan, G., Chopra, J., Kumar, R., Hazra, C., & Sen, R. (2020). Production, partial purification and characterization of a proteoglycan bioemulsifier from an oleaginous yeast. *Bioprocess and Biosystems Engineering, 43*(10), 1747–1759. https://doi.org/10.1007/s00449-020-02361-1

Bonella, S., Raimondo, D., Milanetti, E., Tramontano, A., & Ciccotti, G. (2014). Mapping the hydropathy of amino acids based on their local solvation structure. *Journal of Physical Chemistry B, 118*(24), 6604–6613. https://doi.org/10.1021/jp500980x

Chen, X. Q., Wu, X. F., Zhang, K., Sun, F. J., Zhou, W. L., Wu, Z. Q., & Li, X. T. (2022). Purification, characterization, and emulsification stability of high- and low-molecular-weight fractions of polysaccharide conjugates extracted from green tea. *Food Hydrocolloids, 129*. https://doi.org/10.1016/j.foodhyd.2022.107667

Chylinska, M., Szymanska-Chargot, M., & Zdunek, A. (2016). FT-IR and FT-Raman characterization of non-cellulosic polysaccharides fractions isolated from plant cell wall. *Carbohydrate Polymers, 154*, 48–54. https://doi.org/10.1016/j.carbpol.2016.07.121

Cui, J., Goh, K. K. T., Archer, R., & Singh, H. (2007). Characterisation and bioactivity of protein-bound polysaccharides from submerged-culture fermentation of Coriolus versicolor Wr-74 and ATCC-20545 strains. *Journal of Industrial Microbiology and Biotechnology, 34*(5), 393–402. https://doi.org/10.1007/s10295-007-0209-5

Cui, F.-J., Xin, F., Lei, S., Xin-Yi, Z., Li-Juan, M., & Sun, W.-J. (2024). Recent insights into glucans biosynthesis and engineering strategies in edible fungi. *Critical Reviews in Biotechnology, 44*(7), 1262–1279. https://doi.org/10.1080/07388551.2023.2289341

De, A., Malpani, D., Das, B., Mitra, D., & Samanta, A. (2020). Characterization of an arabinogalactan isolated from gum exudate of odina wodier Roxb.: Rheology, AFM, raman and CD spectroscopy. *Carbohydrate Polymers, 250*, Article 116950. https://doi.org/10.1016/j.carbpol.2020.116950

Di Rienzo, L., Miotto, M., Bo, L., Ruocco, G., Raimondo, D., & Milanetti, E. (2021). Characterizing hydropathy of amino acid side chain in a protein environment by investigating the structural changes of water molecules network. *Frontiers in Molecular Biosciences, 8*, Article 626837. https://doi.org/10.3389/fmolb.2021.626837

Faustino, M., Durao, J., Pereira, C. F., Pintado, M. E., & Carvalho, A. P. (2021). Mannans and mannan oligosaccharides (MOS) from Saccharomyces cerevisiae - A sustainable source of functional ingredients. *Carbohydrate Polymers, 272*, Article 118467. https://doi.org/10.1016/j.carbpol.2021.118467

Ferrero, C. (2017). Hydrocolloids in wheat breadmaking: A concise review. *Food Hydrocolloids, 68*, 15–22. https://doi.org/10.1016/j.foodhyd.2016.11.044

González-Díaz, R. L., Saldarriaga-Hernandez, S., Ramírez-Aguirre, M. D., Guerrero-Higareda, S., García-Cayuela, T., Garcia-Amezquita, L. E., & Carrillo-Nieves, D. (2024). Valorization of brewer's spent grains through Ganoderma lucidum cultivation: Functional food ingredients and bread prototypes. *Lwt, 214*. https://doi.org/10.1016/j.lwt.2024.117131

Guo, Q., Ai, L., & Cui, S. W. (2018). Strategies for structural characterization of polysaccharides. In Q. Guo, L. Ai, & S. Cui (Eds.), *Methodology for structural analysis of polysaccharides* (pp. 1–7). Cham: Springer International Publishing.

Hong, T., Yin, J. Y., Nie, S. P., & Xie, M. Y. (2021). Applications of infrared spectroscopy in polysaccharide structural analysis: Progress, challenge and perspective. *Food Chemistry X, 12*, Article 100168. https://doi.org/10.1016/j.fochx.2021.100168

Huang, S.-q., Li, J.-w., Li, Y.-q., & Wang, Z. (2011). Purification and structural characterization of a new water-soluble neutral polysaccharide GLP-F1-1 from Ganoderma lucidum. *International Journal of Biological Macromolecules, 48*(1), 165–169. https://doi.org/10.1016/j.ijbiomac.2010.10.015

Huang, F., Liu, Y., Zhang, R., Dong, L., Yi, Y., Deng, Y., … Zhang, M. (2018). Chemical and rheological properties of polysaccharides from litchi pulp. *International Journal of Biological Macromolecules, 112*, 968–975. https://doi.org/10.1016/j.ijbiomac.2018.02.054

Iwaki, S., Fu, B. X., & Hayakawa, K. (2023). Behavior of protein aggregates via electrostatic interactions or hydrogen bonds during dough formation. *Journal of Cereal Science, 111*. https://doi.org/10.1016/j.jcs.2023.103683

Jin, W.-J., He, W.-L., Lehner, S., Cheng, X.-W., Gaan, S., & Guan, J.-P. (2024). Edible squid ink proteoglycans as a multifunctional sustainable additive for silk coatings: Fire protection, UV shielding and as a colorant. *Chemical Engineering Journal, 495*. https://doi.org/10.1016/j.cej.2024.153320

Joseph, E., & Singhvi, G. (2019). Chapter 4 - Multifunctional nanocrystals for cancer therapy: A potential nanocarrier. In A. M. Grumezescu (Ed.), *Nanomaterials for drug delivery and therapy* (pp. 91–116). William Andrew Publishing.

Krekora, M., & Nawrocka, A. (2024). Interactions of gliadins with flavonoids and their glycosides studied with application of FT-Raman spectroscopy. *Journal of Cereal Science, 117*. https://doi.org/10.1016/j.jcs.2024.103915

Kuang, J., Xu, K., Dang, B., Zheng, W., Yang, X., Zhang, W., … Huang, J. (2023). Interaction with wheat starch affect the aggregation behavior and digestibility of gluten proteins. *International Journal of Biological Macromolecules, 253*(Pt 4), Article 127066. https://doi.org/10.1016/j.ijbiomac.2023.127066

Li, Z., Gao, W., Liang, J., Fan, H., Yang, Y., Suo, B., & Ai, Z. (2023). Mechanism underlying the weakening effect of beta-glucan on the gluten system. *Food Chemistry, 420*, Article 136002. https://doi.org/10.1016/j.foodchem.2023.136002

Li, J., Zhu, Y., Yadav, M. P., & Li, J. (2019). Effect of various hydrocolloids on the physical and fermentation properties of dough. *Food Chemistry, 271*, 165–173. https://doi.org/10.1016/j.foodchem.2018.07.192

Liu, C. Y., Hu, D. J., Zhu, H., Zhang, Y. Y., Qin, J., Wang, F., … Lv, G. P. (2022). Preparation, characterization and immunoregulatory activity of derivatives of polysaccharide from Atractylodes lancea (thunb.) DC. *International Journal of Biological Macromolecules, 216*, 225–234. https://doi.org/10.1016/j.ijbiomac.2022.06.122

Liu, X., Renard, C., Bureau, S., & Le Bourvellec, C. (2021). Revisiting the contribution of ATR-FTIR spectroscopy to characterize plant cell wall polysaccharides. *Carbohydrate Polymers, 262*, Article 117935. https://doi.org/10.1016/j.carbpol.2021.117935

Liu, X.-Y., Yu, H.-Y., Liu, Y.-Z., Qin, Z., Liu, H.-M., Ma, Y.-X., & Wang, X.-D. (2022). Isolation and structural characterization of cell wall polysaccharides from sesame kernel. *Lwt, 163*. https://doi.org/10.1016/j.lwt.2022.113574

Lopez-Torrez, L., Nigen, M., Williams, P., Doco, T., & Sanchez, C. (2015). Acacia Senegal vs. Acacia seyal gums – Part 1: Composition and structure of hyperbranched plant exudates. *Food Hydrocolloids, 51*, 41–53. https://doi.org/10.1016/j.foodhyd.2015.04.019

Nawrocka, A., Szymanska-Chargot, M., Mis, A., Kowalski, R., & Gruszecki, W. I. (2016). Raman studies of gluten proteins aggregation induced by dietary fibres. *Food Chemistry, 194*, 86–94. https://doi.org/10.1016/j.foodchem.2015.07.132

Nawrocka, A., Szymańska-Chargot, M., Miś, A., Wilczewska, A. Z., & Markiewicz, K. H. (2017). Effect of dietary fibre polysaccharides on structure and thermal properties of gluten proteins – A study on gluten dough with application of FT-Raman spectroscopy, TGA and DSC. *Food Hydrocolloids, 69*, 410–421. https://doi.org/10.1016/j.foodhyd.2017.03.012

Pelton, J. T., & McLean, L. R. (2000). Spectroscopic methods for analysis of protein secondary structure. *Analytical Biochemistry, 277*(2), 167–176. https://doi.org/10.1006/abio.1999.4320

Peng, B., Li, Y., Ding, S., & Yang, J. (2017). Characterization of textural, rheological, thermal, microstructural, and water mobility in wheat flour dough and bread affected by trehalose. *Food Chemistry, 233*, 369–377. https://doi.org/10.1016/j.foodchem.2017.04.108

Qian, J.-Y., Chen, W., Zhang, W.-M., & Zhang, H. (2009). Adulteration identification of some fungal polysaccharides with SEM, XRD, IR and optical rotation: A primary approach. *Carbohydrate Polymers, 78*(3), 620–625. https://doi.org/10.1016/j.carbpol.2009.05.025

Ribotta, P. D., Ausar, S. F., Beltramo, D. M., & León, A. E. (2005). Interactions of hydrocolloids and sonicated-gluten proteins. *Food Hydrocolloids, 19*(1), 93–99. https://doi.org/10.1016/j.foodhyd.2004.04.018

Shao, R. X., Cao, W. D., Huang, X. J., Zhang, N., Ma, L. X., Huang, Y., … Chen, X. Q. (2024). Characterization of emulsions stabilized by aqueous and alkaline extraction of polysaccharide conjugates from bamboo leaves. *Industrial Crops and Products, 219*. https://doi.org/10.1016/j.indcrop.2024.119016

Su, T., Zhang, Y., Du, W., Zeng, J., & Gao, H. (2024). Effect of modified trehalose on regulation of gluten protein structure and steamed bread quality. *International Journal of Biological Macromolecules, 283*(Pt 4), Article 137969. https://doi.org/10.1016/j.ijbiomac.2024.137969

Wang, Y., Han, J., Yue, Y., Wu, Y., Zhang, W., Xia, W., & Wu, M. (2023). Purification, structure identification and immune activity of a neutral polysaccharide from Cynanchum auriculatum. *International Journal of Biological Macromolecules, 237*, Article 124142. https://doi.org/10.1016/j.ijbiomac.2023.124142

Wang, P., Jin, Z., & Xu, X. (2015). Physicochemical alterations of wheat gluten proteins upon dough formation and frozen storage – A review from gluten, glutenin and gliadin perspectives. *Trends in Food Science & Technology, 46*(2, Part A), 189–198. https://doi.org/10.1016/j.tifs.2015.10.005

Wang, H., Ke, L., Ding, Y., Rao, P., Xu, T., Han, H., … Shang, X. (2022). Effect of calcium ions on rheological properties and structure of Lycium barbarum L. polysaccharide and its gelation mechanism. *Food Hydrocolloids, 122*. https://doi.org/10.1016/j.foodhyd.2021.107079

Wang, X., Liang, Y., Wang, Q., Zhang, X., & Wang, J. (2021). Effect of low-sodium salt on the physicochemical and rheological properties of wheat flour doughs and their respective gluten. *Journal of Cereal Science, 102*. https://doi.org/10.1016/j.jcs.2021.103371

Wang, K. Q., Luo, S. Z., Zhong, X. Y., Cai, J., Jiang, S. T., & Zheng, Z. (2017). Changes in chemical interactions and protein conformation during heat-induced wheat gluten gel formation. *Food Chemistry, 214*, 393–399. https://doi.org/10.1016/j.foodchem.2016.07.037

Wang, P., Zou, M., Gu, Z., & Yang, R. (2018). Heat-induced polymerization behavior variation of frozen-stored gluten. *Food Chemistry, 255*, 242–251. https://doi.org/10.1016/j.foodchem.2018.02.047

Wieser, H., Koehler, P., & Scherf, K. A. (2022). Chemistry of wheat gluten proteins: Qualitative composition. *Cereal Chemistry, 100*(1), 23–35. https://doi.org/10.1002/cche.10572

Xiong, S., Tao, P., Yu, Y., Wu, W., Li, Y., Chen, G., … Yang, H. (2024). Effect of Polygonatum cyrtonema hua polysaccharides on gluten structure, in vitro digestion and shelf-life of fresh wet noodle. *International Journal of Biological Macromolecules, 279*(Pt 4), Article 135475. https://doi.org/10.1016/j.ijbiomac.2024.135475

Xu, Z., Ma, Y., Hong, T., Shao, G., Lv, L., Xu, D., … Xu, X. (2024). Effect of liquid fermented Chinese edible Ganoderma lucidum fungus on wheat bread: A quality improver and staling inhibitor. *Food Control, 155*. https://doi.org/10.1016/j.foodcont.2023.110060

Xu, Z., Xu, D., Jin, Y., Zhang, H., Wu, F., Zhang, J., & Xu, X. (2025). Processing properties of wheat dough mediated by proteoglycan extracted from the liquid fermented Ganoderma lucidum. *Food Bioscience, 63*. https://doi.org/10.1016/j.fbio.2024.105602

Yin, B., Wang, C., Liu, Z., & Yao, P. (2017). Peptide-polysaccharide conjugates with adjustable hydrophilicity/hydrophobicity as green and pH sensitive emulsifiers. *Food Hydrocolloids, 63*, 120–129. https://doi.org/10.1016/j.foodhyd.2016.08.028

Zhang, H., Liu, S., Feng, X., Ren, F., & Wang, J. (2023). Effect of hydrocolloids on gluten proteins, dough, and flour products: A review. *Food Research International, 164*, Article 112292. https://doi.org/10.1016/j.foodres.2022.112292

Zhang, M., Ruobing, J., Meng, M., Tianbao, Y., Qingjie, S., & Li, M. (2023). Versatile wheat gluten: Functional properties and application in the food-related industry. *Critical Reviews in Food Science and Nutrition, 63*(30), 10444–10460. https://doi.org/10.1080/10408398.2022.2078785

Zhou, Y., Dhital, S., Zhao, C., Ye, F., Chen, J., & Zhao, G. (2021). Dietary fiber-gluten protein interaction in wheat flour dough: Analysis, consequences and proposed mechanisms. *Food Hydrocolloids, 111*. https://doi.org/10.1016/j.foodhyd.2020.106203

Zhou, Y., Liu, W., Cao, W., Cheng, Y., Liu, Z., & Chen, X. (2023). Effect of hydrophobic property on antibacterial activities of green tea polysaccharide conjugates against Escherichia coli. *International Journal of Biological Macromolecules, 253*(Pt 1), Article 126583. https://doi.org/10.1016/j.ijbiomac.2023.126583

Zhou, H., Liu, G., Huang, F., Wu, X., & Yang, H. (2014). Improved production, purification and bioactivity of a polysaccharide from submerged cultured Ganoderma lucidum. *Archives of Pharmacal Research, 37*(12), 1530–1537. https://doi.org/10.1007/s12272-014-0391-8